JOURNAL OF GEOPHYSICAL RESEARCH, VOL. 112, D19105, doi:10.1029/2006JD008317, 2007

A method to measure Kr/N_2 ratios in air bubbles trapped in ice cores and its application in reconstructing past mean ocean temperature

Melissa A. Headly[1] and Jeffrey P. Severinghaus[1]

Received 5 December 2006; revised 20 June 2007; accepted 6 July 2007; published 10 October 2007.

[1] We describe a new method for precise measurement of Kr/N_2 ratios in air bubbles trapped in ice cores and the first reconstruction of atmospheric Kr/N_2 during the last glacial maximum (LGM) ~20,000 years ago. After gravitational correction, the Kr/N_2 record in ice cores should represent the atmospheric ratio, which in turn should reflect past ocean temperature change due to the dependence of gas solubility on temperature. The increase in krypton inventory in the glacial ocean due to higher gas solubility in colder water causes a decrease in the atmospheric inventory of krypton. Assuming Kr and N_2 inventories in the ocean-atmosphere system are conserved, we use a mass balance model to estimate a mean ocean temperature change between the LGM and today. We measured Kr/N_2 in air bubbles in Greenland (GISP2) ice from the late Holocene and LGM, using the present atmosphere as a standard. The late Holocene $\delta Kr/N_2$ means from two sets of measurements are not different from zero ($+0.07 \pm 0.30‰$ and $-0.14 \pm 0.93‰$), as expected from the relatively constant climate of the last millennium. The mean $\delta Kr/N_2$ in air bubbles from the LGM is $-1.34 \pm 0.37‰$. Using the mass balance model, we estimate that the mean temperature change between the LGM ocean and today's ocean was $2.7 \pm 0.6°C$. Although this error is large compared to the observed change, this finding is consistent with most previous estimates of LGM deep ocean temperature based on foraminiferal $\delta^{18}O$ and sediment pore water $\delta^{18}O$ and chlorinity.

Citation: Headly, M. A., and J. P. Severinghaus (2007), A method to measure Kr/N_2 ratios in air bubbles trapped in ice cores and its application in reconstructing past mean ocean temperature, *J. Geophys. Res.*, *112*, D19105, doi:10.1029/2006JD008317.

1. Introduction

[2] Deep ocean temperature is a fundamental parameter of the climate system, but its past variations remain poorly known despite decades of research. This is due mainly to the inherent ambiguity of oxygen isotope ($\delta^{18}O$) records from benthic foraminifera, which are affected by both temperature and ice volume [*Shackleton*, 2000]. In an effort to separate the temperature from the ice volume signal in the benthic $\delta^{18}O$ record, *Schrag et al.* [1996] measured the $\delta^{18}O$ in sediment pore waters. These pore water studies provided single estimates of deep ocean cooling at the last glacial maximum (LGM) at several different core sites. Their conclusion was that the deep ocean temperature was ~4°C cooler during the LGM than it is today, near the freezing point of seawater [*Schrag et al.*, 1996]. However, this result only applies to the local temperature at the sediment core sites. Changes in local hydrography can obscure the global signal [*Adkins and Schrag*, 2001]. The deep ocean is heterogeneous from place to place, limiting the representativeness of these sites. Others have also tried to reconstruct deep ocean temperature by using benthic Mg/Ca ratios [*Martin et al.*, 2002] and regressions of benthic $\delta^{18}O_{calcite}$ versus reconstructed relative sea level from fossil corals [*Waelbroeck et al.*, 2002; *Cutler et al.*, 2003]. Like Schrag et al.'s study, these are estimates of local deep ocean temperature. Furthermore, Mg/Ca ratios in benthic foraminifera can be affected by diagenesis, in addition to temperature [*Martin et al.*, 2002].

[3] We use $\delta Kr/N_2$ measured in air bubbles in ice cores as a new proxy for past ocean temperature variations. The dissolved concentration of krypton in seawater varies with ocean temperature, causing a complementary shift in its atmospheric abundance [*Craig and Weins*, 1996]. Krypton is measured as a ratio to nitrogen concentration because nitrogen does not respond as sensitively to ocean temperature because of its low solubility in water, and direct measurement of the absolute krypton inventory is impractical. Molecular weight primarily governs the solubility of gases in solution, so krypton is more soluble than the lighter gases. Solubility for gases increases with lower water temperatures, and its dependence on temperature becomes more pronounced at lower temperatures. The relative fractions of krypton in the present-day atmosphere and ocean are approximately 98% and 2%, respectively, and 99.5% and 0.5% for nitrogen [*Schlesinger*, 1997; *Weiss and Kyser*, 1978; *Weiss*, 1970].

[4] The $\delta Kr/N_2$ measurements should provide an estimate of whole-ocean average temperature change because Kr and N_2 are well mixed in the atmosphere. These atmospheric gases integrate global solubility-driven air-sea fluxes. Ad-

[1]Scripps Institution of Oceanography, University of California, San Diego, La Jolla, California, USA.

0148-0227/07/2006JD008317$09.00

ditionally, $\delta Kr/N_2$ measurements in ice cores have the potential to resolve a time series of ocean temperature change because they provide discrete samples of the past atmosphere, in contrast to the pore water studies which are limited to a single (LGM) point.

2. Hypothesis and Conceptual Model

[5] In order to interpret the $\delta Kr/N_2$ measured in ice cores as a proxy of past mean ocean temperature, we calculate expected paleoatmospheric concentrations of Kr and N_2 using a conceptual model of the ocean-atmosphere system. A mass balance approach is used, conserving the total inventory of Kr and N_2 in the ocean-atmosphere system between the LGM and today, as shown in (1) and (2) below:

$$\begin{aligned} Kr_{\text{present ocean}} + Kr_{\text{present atmosphere}} &= Kr_{\text{total}} \\ &= Kr_{\text{LGM ocean}} + Kr_{\text{LGM atmosphere}} \end{aligned} \tag{1}$$

$$\begin{aligned} N_{2\,\text{present ocean}} + N_{2\,\text{present atmosphere}} &= N_{2\,\text{total}} \\ &= N_{2\,\text{LGM ocean}} + N_{2\,\text{LGM atmosphere}}. \end{aligned} \tag{2}$$

By conservation of mass, the difference between the LGM ocean inventory and today's inventories must have been taken up by the LGM atmosphere, as these gases are inert or nearly so, and sources and sinks to the ocean-atmosphere system are negligible on the timescale of interest. We assume that nitrogen fixation and denitrification have a negligible effect on the total N_2 inventory. This assumption is supported by the observation that the entire denitrifiable inventory of nitrogen represents less than 0.01% of the atmospheric inventory [*Schlesinger*, 1997].

[6] For clarity, we note that gas content and heat content in the ocean are set at the surface outcrop where air-sea equilibration occurs [*Hamme and Emerson*, 2002]. As a water parcel moves through the ocean, these quantities are conserved. There is no time lag of one versus the other. Therefore the amount of Kr and N_2 in the ocean is indicative of the average temperature of the ocean at any point in time, making the consideration of ocean mixing time in our calculation unnecessary.

[7] The current oceanic Kr and N_2 inventories ($Kr_{\text{present ocean}}$ and $N_{2\text{present ocean}}$, respectively) are estimated by using a multibox model of the ocean that incorporates the distribution of observed temperatures. The ocean is divided into 1° latitude × 1° longitude boxes with varying depth segments (ocean depth is divided into 33 depth intervals). $Kr_{\text{present ocean}}$ and $N_{2\text{present ocean}}$ are calculated using the krypton solubility algorithms of *Weiss and Kyser* [1978], and those for nitrogen of *Weiss* [1970]. Dissolved gases in the ocean are assumed to be at equilibrium with the atmosphere. This assumption may not be strictly correct [*Hamme and Severinghaus*, 2007], but it will not affect our calculation substantially. Ocean temperature data used in our calculations are given as the mean temperature of each grid box used in the model [*Levitus*, 1994]. Salinity is assumed to be 35 psu in all boxes.

[8] The Kr and N_2 solubilities (in μg/mol) are multiplied by the mass of the ocean in each grid box in order to convert them to Kr and N_2 inventories in moles, as shown in (3) and (4). The Levitus density data (ρ) are multiplied by the grid box's volume (V) to calculate the mass of each grid box. The model does not include bottom topography, and therefore does not take into account varying bottom depths in calculating ocean volume. Rather, data taken at depths deviating from the 33 standard depth levels are interpolated from the observed depth to a standard depth. The standard depths are then used in calculating ocean volume. The inventories of Kr ($Kr_{\text{present ocean}}$) and N_2 ($N_{2\text{present ocean}}$) for n grid boxes are calculated as shown below:

$$Kr_{\text{present ocean}} = \sum_{i=1}^{n} [G]_{Kr}(T,S) \times \rho \times V \tag{3}$$

$$N_{2\,\text{present ocean}} = \sum_{i=1}^{n} [G]_{N_2}(T,S) \times \rho \times V. \tag{4}$$

The Kr and N_2 in each box are summed to obtain a whole-ocean inventory of Kr and N_2 in today's ocean ($Kr_{\text{present ocean}}$ and $N_{2\text{present ocean}}$), which are used in equations (1) and (2). We find $Kr_{\text{present ocean}}$ and $N_{2\text{present ocean}}$ to be 4.35×10^{12} moles and 6.52×10^{17} moles, respectively.

[9] The second terms in equations (1) and (2), $Kr_{\text{present atmosphere}}$ and $N_{2\text{present atmosphere}}$, are calculated by multiplying the known mole fraction of these gases in today's atmosphere by the total moles of air, 1.77×10^{20} moles (calculated using the mass of the atmosphere and the molecular weight of dry air from *Schlesinger* [1997]). The calculated atmospheric Kr and N_2 inventories are 2.02×10^{14} moles and 1.38×10^{20} moles, respectively.

[10] The first terms on the right side of equations (1) and (2), $Kr_{\text{LGM ocean}}$ and $N_{2\text{LGM ocean}}$, are calculated using the ocean box model described above. The temperature variable used to calculate the present oceanic inventories is reduced by 0.5°C to 6.0°C to simulate a wide range of mean ocean temperature changes between the LGM and today. Higher salinity of the LGM ocean is also included in the model, assuming an LGM salinity of 36 psu [*Adkins and Schrag*, 2001]. The LGM ocean model also accounts for the reduction in sea level (and thus ocean volume) at that time. Measurements from past coral terraces indicate that sea level was ~120 m lower during the LGM [*Fairbanks*, 1989], which corresponds to a 3% decrease in ocean volume. Another expected consequence of lower sea level during the LGM is an increase in sea level barometric pressure. This pressure increase is due to the displacement of water from the ocean and onto land in the form of ice sheets, decreasing surface pressure over land, and increasing it over the lower sea level. We estimate the increase in sea level pressure resulting from a 120 m decrease in sea level as follows:

$$p/p_o = e^{-z/H}. \tag{5}$$

[11] The scale height of the atmosphere (H) is assumed to be 7600 m in deep water formation regions, and sea level

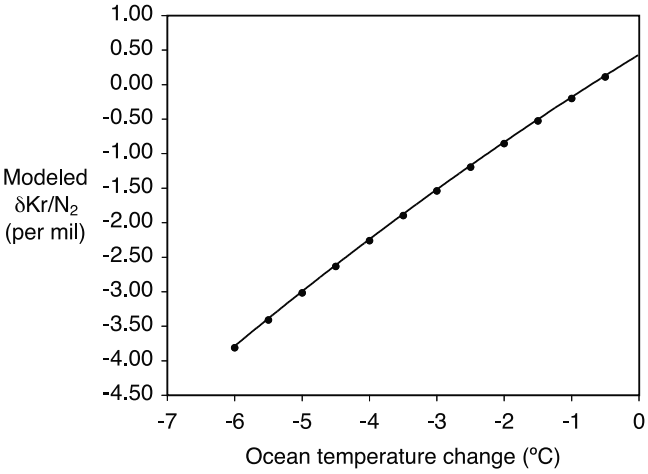

Figure 1. Modeled $\delta Kr/N_2$ versus ocean temperature change between now and the LGM. Modeled $\delta Kr/N_2$ is positive at $-0.5°C$ because of smaller ocean volume during the LGM. Second-order polynomial fit to points: $y = -0.0175x^2 + 0.5989x + 0.4146$.

height (z) at the LGM is -120 m (in reference to today's sea level). This yields 1.0159 for p/p_o, the ratio of LGM sea level pressure (at $z = -120$ m), to the pressure at sea level today (at $z = 0$). Henry's law states that partial pressure and dissolved concentration of a gas are directly proportional, so the Kr and N_2 oceanic inventories would increase by 1.59% because of higher sea level pressure during the LGM. This calculation neglects the fact that ice sheets displace air at slightly higher elevations (and thus lower air densities) than does seawater, although this fact is largely compensated by the lower density of ice than water. This calculation also neglects possible synoptic changes in sea level barometric pressure, which are currently unknown.

[12] Other potential factors that could influence the amount of Kr and N_2 in the LGM ocean include changes in wind patterns and diapycnal mixing. It is widely accepted that winds were stronger during the LGM, as suggested by increased dust deposits in ice cores [*Crowley and North*, 1991]. Stronger winds or changes in wind patterns during the LGM could alter the amount of bubble entrainment, or injection, into ocean waters. *Hamme and Emerson* [2002] have shown that air bubble injection preferentially increases the abundance of less soluble gases (including N_2) in the ocean. Therefore an increase in bubble injection would cause our measurements to be biased toward lower $\delta Kr/N_2$ values, and an underestimation of ocean temperature change. Bubble injection is unlikely to have a significant influence on our measurements. The effect of doubling bubble injection would change $\delta Kr/N_2$ by $\sim$0.2‰, which is less than measurement error (0.37‰) [*Hamme and Severinghaus*, 2007]. Likewise, although diapycnal mixing is suggested to have changed between the LGM and today [*Watson and Garbato*, 2006; *Egbert et al.*, 2004], it is unlikely to affect our measurements significantly. Diapycnal mixing within the ocean, isolated from the surface, would have no affect on atmospheric $\delta Kr/N_2$ because we are concerned with Kr and N_2 abundances, rather than their saturation state. In a case where diapycnal mixing creates an intermediate depth water parcel that outcrops at the surface, the effect on $\delta Kr/N_2$ values should only be $\sim 0.1-0.2$‰ at most, which is within our measurement error.

[13] The last terms in equations (1) and (2), $Kr_{LGM\ atmosphere}$ and $N_{2LGM\ atmosphere}$, are measured in the air bubbles in ice from the LGM as the ratio, Kr/N_2. $Kr_{LGM\ atmosphere}$ and $N_{2LGM\ atmosphere}$, are also modeled using the mass balance ocean-atmosphere model, and compared to the measurements to interpret the results. The total amount of Kr and N_2 in the ocean and atmosphere together are constant on these timescales, so the increase in LGM ocean inventories due to ocean temperature change must cause a resultant decrease in LGM atmospheric inventories. Therefore it follows from (1) and (2) that

$$Kr_{LGM\,atmosphere} = Kr_{total} - Kr_{LGM\,ocean} \tag{6}$$

$$N_{2\,LGM\,atmosphere} = N_{2\,total} - N_{2\,LGM\,ocean}, \tag{7}$$

where Kr_{total} and N_{2total} are the sum of today's atmosphere and ocean inventories of each gas. The modeled Kr and N_2 in the LGM atmosphere vary with mean ocean temperature change (Figure 1). In this study, the Kr/N_2 ratio is expressed in the customary delta notation, which describes the deviation of the sample Kr/N_2 from a standard Kr/N_2 ratio:

$$\delta Kr/N_2 = \left[\left(Kr/N_{2\,sample}/Kr/N_{2\,standard}\right) - 1\right] \times 10^3\ ‰. \tag{8}$$

The standard used is the ratio of Kr/N_2 present in today's atmosphere (from samples taken on the SIO pier in La Jolla, CA).

3. Analytical Technique

[14] The analytical approach used in this study is based primarily on the techniques outlined by *Severinghaus et al.* [2003] and *Sowers et al.* [1989]. Ice samples of approximately 50–60 g are cut using a band saw in a walk-in freezer, kept at $-20°C$. Edges (5 mm) of the ice sample are removed using a band saw to expose fresh ice surfaces. The long axis of the sample is parallel to the ice core, so that each sample is typically an average of several annual layers. The piece is then cut into 2–4 smaller pieces to fit into the extraction vessel. The extraction vessel is a custom-made 400-cm^3 glass vessel. The ice sample and two glass-covered magnetic stir bars are lowered into the extraction vessel with chilled tongs. Two stir bars were found to be more effective than one in extracting krypton during the transfer of gas from the extraction vessel to the sample dip tube (Figure 2).

[15] The extraction vessel is then attached to the vacuum line using a gold-plated copper conflat gasket, and the ambient air is pumped out of the vessel for 40 min. The extraction vessel is kept in an ethanol dewar at $-20°C$ during the pump down. Sublimation and subsequent water vapor flow during pumping effectively remove any gases adsorbed onto the ice [*Severinghaus et al.*, 2003]. The total pressure is measured to monitor outgassing at 5 min and at the end of the 40 min of pumping, at which point the pressure should reduce to the vapor pressure of water over ice at $-20°C$. After 40 min, the extraction vessel is sealed,

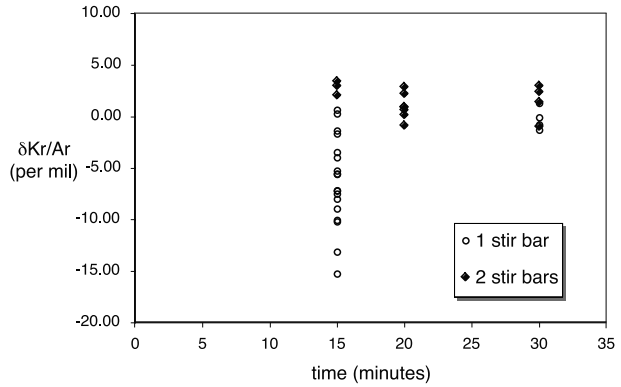

Figure 2. Test results from development of gas transfer technique for δKr/Ar. δKr/Ar is plotted versus time. The number of stir bars used to agitate the meltwater during gas transfer is indicated.

and the ice sample is melted using a warm bath, releasing the trapped gas in the ice. The trapped gas is transferred for 20 min through a -100°C glass water trap. The gas transfer is accomplished by freezing the sample at 4 K in a dip tube that has been lowered into a tank of liquid helium. Connections are made using Ultratorr fittings with Viton O-rings. During transfer, two stir bars are used to agitate the melted ice to ensure complete extraction of krypton, which is difficult to degas because of its high solubility. The residual pressure after the 20-min transfer is checked to ensure complete transfer. The gas in the dip tube comprises approximately 4 standard cm^3.

[16] We have modified the gas extraction method outlined by *Severinghaus et al.* [2003] to ensure complete extraction of krypton. We varied several parameters to determine the optimal gas extraction and transfer conditions. These parameters include transfer time through the water trap into the sample tube in liquid He, the number of magnetic stir bars used, and temperature of the glass vessel (which is maintained with a warm bath during the transfer). We interpret the degree of Kr extracted in terms of the δKr/Ar of late Holocene ice in reference to the current atmosphere. Ideally, the δKr/Ar measurement should be 0‰ because neither krypton nor argon's atmospheric abundance should have changed significantly during the late Holocene. Because of potential Ar gas loss out of the ice, we expected the actual δKr/Ar measured in Holocene ice to be slightly higher than 0‰ (*Severinghaus et al.* [2003] found +4‰). Kr/N_2 measurement (which apparently is not affected by gas loss [*Severinghaus and Battle*, 2006]) was not yet possible at the time of this method development.

[17] The δKr/Ar results from the gas extraction tests are shown in Figure 2. The most complete extraction of krypton from the melted ice occurred with longer transfer times and the use of two stir bars. A transfer time of at least 20 min resulted in higher measured δKr/Ar values, which are indicative of a more complete krypton extraction. An additional stir bar (two stir bars total), used to increase the agitation of the meltwater and encourage outgassing, likewise appeared to increase the δKr/Ar values. We also tested the addition of a warm bath surrounding the glass vessel containing the ice during transfer, which raised the temperature of the melted ice and therefore lowered krypton's solubility in the meltwater. The presence of the warm bath did not noticeably increase the observed δKr/Ar; however, it is possible that gas occlusion in the water trap (discussed below) may mask enhanced extraction because of increased flow of water vapor.

[18] Another consideration is the possibility that Kr might be unintentionally trapped in the water trap during gas transfer by gas occlusion. Previous work has shown that when a large amount of water vapor is transferred through a water trap, a gas can become trapped by occlusion under the freezing water vapor (W. Jenkins, personal communication, 2007). Our control data from ice from the late Holocene shows no change in $\delta Kr/N_2$ within error (Figure 3), so it is unlikely that occlusion preferentially affects either Kr or N_2. Nevertheless, we have tested for the presence of this effect by heating up the water trap after gas extraction and transfer. The occluded gas subsequently released from the water trap ($\sim$0.005% of the total sample pressure) was then transferred to the dip tube (already containing the original sample) through a second water trap. Gas occlusion in the water trap in this second transfer is less likely because of lower water vapor flow than in the original transfer. $\delta Kr/N_2$ results from this "test" sample of late Holocene ice showed no significant difference from the rest of our data set from the late Holocene ($\delta Kr/N_2$ values were within error of 0‰). Therefore it appears that gas occlusion is not significantly affecting our measurements.

[19] After the gas extraction, the dip tube is removed from the liquid He tank. It then warms to room temperature and is allowed to homogenize before mass spectrometry. Sample tube homogenization time was estimated in a separate experiment by transferring an aliquot of an air standard gas of $\sim$4 cm^3 into a sample dip tube, letting it homogenize for various amounts of time after removal from the liquid He tank, and then running it against the standard gas itself on a Finnigan Delta Plus XP mass spectrometer. Tested homogenization times ranged from 30 min to 18 hours. The measured $\delta^{15}N$, $\delta^{18}O$, $\delta O_2/N_2$, and $\delta Ar/N_2$ all approached 0‰ (the expected value for the standard gas versus itself) at 2 hours homogenization time (Figure 4). We therefore chose 2 hours to be the minimum homogenization time for a sample after it is removed from liquid He. This homogenization time applies to the sample tube containing $\sim$4 cm^3 of air extracted from the ice samples.

[20] After at least 2 hours of homogenization, the gas in the sample dip tube is analyzed on a Finnigan Delta Plus XP mass spectrometer to determine the $\delta^{15}N$, $\delta^{18}O$, $\delta O_2/N_2$, and $\delta Ar/N_2$ of the sample. The standard gas, dry La Jolla air from a laboratory tank at approximately 50 psig, is expanded into a 1-cm^3 aliquot volume for 6 min. Then both sample and standard gas aliquots are expanded into their respective bellows for 6 min. The mass spectrometer measures the delta values in blocks of 16 cycles consisting of 16 s integrations. We use 2 blocks of measurements, giving a total of 32 measurements per sample. The $\delta Ar/N_2$ measurement is used later to directly calculate the $\delta Kr/N_2$ value:

$$\delta Kr/N_2 = \left\{ \left[\left(\frac{\delta^{84}Kr/^{36}Ar}{10^3} + 1 \right) \Big/ \left(\frac{\delta^{40}Ar/^{36}Ar}{10^3} + 1 \right) \times \left(\frac{\delta^{40}Ar/^{28}N_2}{10^3} + 1 \right) \right] - 1 \right\} \times 10^3‰. \quad (9)$$

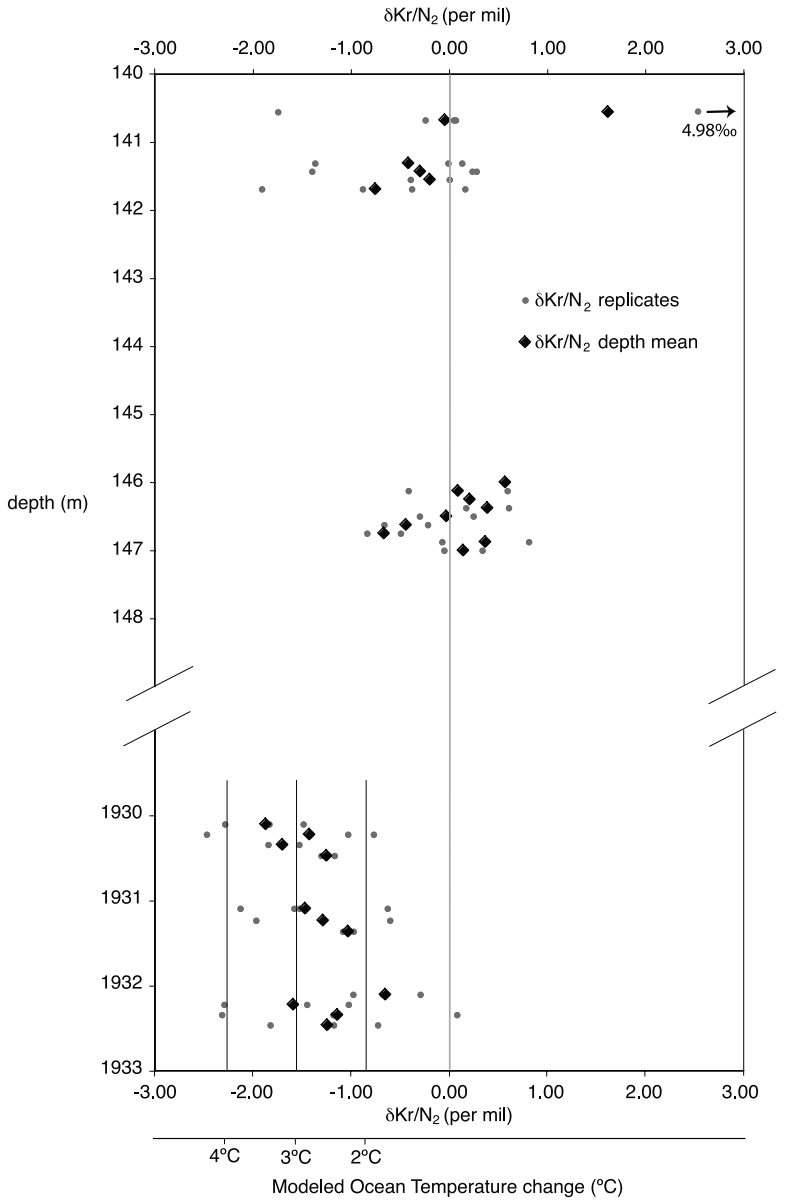

Figure 3. GISP2 ice core depth plotted versus $\delta Kr/N_2$. Vertical axis is not to scale. Long shaded vertical line denotes $\delta Kr/N_2 = 0‰$. Small shaded circles are individual replicates at each depth, and bold solid diamonds are the mean values for each depth. Late Holocene $\delta Kr/N_2$ are shown for depths ~140–142 m and ~146–147 m. Means are +0.07 ± 0.30‰ (n = 16) for one set of measurements (~146 m), and −0.14 ± 0.93‰ (n = 17) for another set of measurements (~140.5–142 m). Both measurements are within error of 0‰. Measurement error is reported as the pooled standard deviation (equation (16)) divided by the square root of the number of replicates. LGM $\delta Kr/N_2$ measurements are shown in the bottom portion (at 1930–1933 m depths). The mean $\delta Kr/N_2$ at in this depth range is −1.34 ± 0.37‰. Short vertical lines are the modeled $\delta Kr/N_2$ resulting from a 2°, 3°, and 4°C ΔT mean ocean temperature change.

The $\delta^{15}N$ of N_2 is used as an additional indicator of gravitational fractionation (the other being $\delta^{40}Ar/^{36}Ar$), and to identify thermal fractionation [*Severinghaus and Brook*, 1999]. The $\delta^{18}O$ of O_2 may be used for chronological purposes [*Sowers and Bender*, 1995], and the $\delta O_2/N_2$ is used to indicate gas loss and to correct for an artifact known as the "chemical slope" [*Severinghaus et al.*, 2003], which is described in next section. Typical standard deviations of the reported values for the $\delta^{15}N$, $\delta^{18}O$, $\delta O_2/N_2$, and $\delta Ar/N_2$ measurements in ice cores are 0.008‰, 0.014‰, 0.50‰, and 0.40‰, respectively. CO_2 and water vapor in the sample and standard gases are monitored for possible isobaric interference [*Sowers et al.*, 1989].

[21] The sample gas is then recovered from the Delta XP mass spectrometer for noble gas measurements on the Finnigan MAT 252 mass spectrometer. Remaining gas in the inlet and the sample bellows of the Delta XP mass spectrometer is quantitatively refrozen into another dip tube

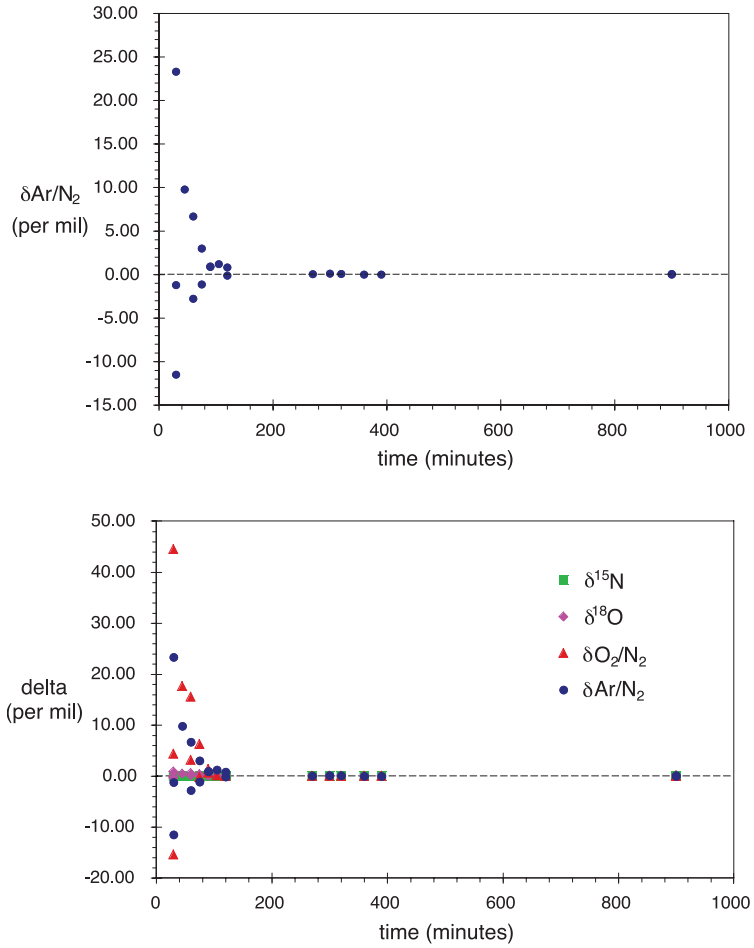

Figure 4. (top) Measured $\delta Ar/N_2$ plotted versus homogenization time. (bottom) All measured gases on the Delta XP ($\delta^{15}N$, $\delta^{18}O$, $\delta Ar/N_2$, and $\delta O_2/N_2$) versus homogenization time. Note that all gases approach 0‰ (their expected value) after 2 hours.

in liquid helium. We have tested this "refreezing" step to determine if any significant fractionation occurs in the subsequent noble gas measurements. We measured two sets of samples: one consisting of gas samples that were "refrozen" from the mass spectrometer, and one set that were "blanks," identical gas samples that were not subject to the refreezing step. The gas used for these tests was a laboratory standard tank filled with dry La Jolla air at 50 psig. Both sets of samples were measured on the Finnigan MAT 252 for $\delta^{40}Ar/^{36}Ar$ (hereafter referred to as $\delta^{40}Ar$) and $\delta Kr/Ar$. The "blanks" and refrozen samples were run alternately. Using a Student t-test, measured values of $\delta^{40}Ar$ and $\delta Kr/Ar$ in the two sets of data were compared to each other.

[22] The first set of tests, done in September 2003, showed a marginally significant difference at the 95% confidence level in the $\delta Kr/Ar$ measurement between the "blanks" and refrozen samples ($t = 2.170$), but no significant difference in the $\delta^{40}Ar$ measurements ($t = 1.340$). The mean and standard deviations for $\delta Kr/Ar$ "blanks" and refrozen samples were 29.97 ± 0.25‰ and 30.19 ± 0.25‰, respectively, and those of $\delta^{40}Ar$ were 1.907 ± 0.020‰ and 1.915 ± 0.011‰, respectively. A subsequent set of testing in May 2004 revealed that this difference had been caused by a leaky valve in the Delta XP mass spectrometer. When the sample gases were not exposed to this valve, the two sets of measurements were not significantly different at the 95% confidence level ($t = 0.046$ and 0.496 for $\delta Kr/Ar$ and $\delta^{40}Ar$, respectively). The means and standard deviations of "blanks" and refrozen samples were 29.30 ± 0.40‰ and 29.32 ± 0.84‰, respectively, for $\delta Kr/Ar$, and 1.885 ± 0.036‰ and 1.869 ± 0.064‰ for $\delta^{40}Ar$.

[23] During the May analysis, two samples were excluded owing to anomalously low $\delta^{40}Ar$ values. These $\delta^{40}Ar$ values were both measured on 3 May 2004. The first sample measured that day had a $\delta^{40}Ar$ value of 1.189‰, with subsequent sample $\delta^{40}Ar$ values climbing steadily throughout the day, until reaching a typical $\delta^{40}Ar$ value (~1.8–1.9‰) on the following day. The cause of the low $\delta^{40}Ar$ values therefore appeared to be linked to a problem with the mass spectrometer, possibly a small contamination that occurred before starting measurements on 3 May, and then reduced in intensity throughout the day due to pumping of the mass spectrometer source and inlet.

[24] After the sample is recovered by this refreezing step, the sample gas is exposed to a Zr/Al getter at 900°C to remove the N_2, O_2, and other reactive gases, following *Severinghaus et al.* [2003]. The remaining noble gases are frozen into a dip tube at 4 K for 3 min. Ultrahigh purity tank

N_2 equal to 10× the noble gas pressure in the vacuum line (precision of 0.001 torr) is added to the sample to add bulk, which is necessary to maintain pressure for viscous flow during mass spectrometry. The N_2 is frozen into the same dip tube at 4 K for 3 min. The accuracy of the N_2 addition is evaluated by measuring sample N_2/Ar versus the N_2/Ar in the working standard (which also has a N_2/Ar ratio of 10). The average δN_2/Ar values in this data set were ~2‰. After 40 min of homogenization, δ^{40}Ar, δKr/Ar, and δXe/Ar in the sample are measured on a Finnigan MAT 252 mass spectrometer, with respect to the working standard. The δ^{40}Ar, δKr/Ar, and δXe/Ar are analyzed on the mass spectrometer as described by *Severinghaus et al.* [2003]. Typical standard deviations of δ^{40}Ar, δKr/Ar, and δXe/Ar in replicate ice core measurements at a given depth are 0.020‰, 0.70‰, and 3.5‰, respectively.

[25] The δKr/N_2 is calculated using the δKr/Ar and δ^{40}Ar measured on the MAT 252, and the δAr/N_2 measured on the Delta XP (equation (9)). The δ^{40}Ar measurement is also used to correct for gravitational settling, as described in a subsequent section.

3.1. Corrections

[26] The sample and standard gases are not necessarily the same size when expanded into the mass spectrometer bellows. During mass spectrometry, the pressure of a smaller gas sample typically falls faster than that of a bigger sample. This pressure imbalance can artifactually affect the measured values because of machine nonlinearity. To minimize this effect, we start the smaller sample at a higher pressure than the bigger sample at the beginning of the mass spectrometer run. We also make a correction for the actual pressure difference between sample and standard gases by scaling the pressure difference by the empirically determined Pressure Imbalance Sensitivity (PIS) (equations (10) and (11)), as described by *Severinghaus et al.* [2003].

$$\delta_{\text{corrected}} = \delta_{\text{measured}} - \text{PIS}\Delta_{\text{pressure}}, \tag{10}$$

$$\Delta_{\text{pressure}} = {}^{36}\text{Ar}_{\text{sample}}/{}^{36}\text{Ar}_{\text{standard}} - 1(\text{MAT 252}), \tag{11a}$$

$$\Delta_{\text{pressure}} = {}^{28}\text{N}_{2\,\text{sample}} - {}^{28}\text{N}_{2\,\text{standard}}(\text{Delta XP})\ \ (\text{volts}). \tag{11b}$$

[27] Another correction is made for the sensitivity of the measured isotopic ratios, δ^{40}Ar, δ^{15}N, and δ^{18}O, to certain elemental ratios. We call this the "chemical slope" correction [*Severinghaus et al.*, 2003]. The δ^{40}Ar measurement is sensitive to changes in the N_2/Ar ratio because the relative ionization efficiencies of ^{40}Ar and ^{36}Ar are affected by differences in N_2/Ar between the sample and standard gases. This effect is probably due to ion-molecule reactions in the mass spectrometer source, but is not well understood. We make this correction empirically following *Severinghaus et al.* [2003]. Varying amounts of ultrapure N_2 are added to an aliquot of the working standard gas, and then it is run on the mass spectrometer versus the standard gas. The pressure-corrected δ^{40}Ar of the standard versus itself should be 0‰, so any deviation from that value can be attributed to the chemical slope. The correction for the chemical slope is calculated as follows:

$$\delta\,{}^{40}\text{Ar}/{}^{36}\text{Ar}_{\text{slope corrected}} = \delta\,{}^{40}\text{Ar}/{}^{36}\text{Ar}_{\text{pressure corrected}} - [\text{chemical slope}] \times \delta\text{N}_2/\text{Ar}_{\text{measured}}. \tag{12}$$

The chemical slope is usually calculated at the beginning of a set of measurements. The chemical slope used in this study was y = 0.000446x (R^2 = 0.97). The chemical slope corrections to the δ^{40}Ar measurements were <0.005‰, which are small compared to the signal size (~1.200–1.800‰) and measurement error (0.020‰). The mass spectrometer used for our measurements is tuned to optimize linearity, and thus minimize chemical slope [*Severinghaus et al.*, 2003]. The chemical slope does not change more than 20% over time and during the source filament lifetime, which limits the possible error under the most extreme scenario to 0.001‰.

[28] A chemical slope correction is also made to the δ^{15}N measurement, which can be affected by the $\delta O_2/N_2$ and the δCO_2 values. A difference between the sample and standard CO_2 abundance can cause differential isobaric interference of CO^+ with N_2^+ [*Sowers et al.*, 1989]. The ion $^{13}CO^+$ has a mass of 29, which is the same as the mass measured for the δ^{15}N of N_2 (^{15}N^{14}N). The δ^{18}O measurement is also corrected for differences in $\delta N_2/O_2$. All chemical slope corrections are made as described above for δ^{40}Ar.

3.2. Normalization to Atmosphere

[29] Ice core δKr/N_2 values are measured on the mass spectrometer in reference to working standards made from commercially available gases or dry air from the SIO pier [*Severinghaus et al.*, 2003]. Because the isotopic values of the working standards may be arbitrary, we normalize the ice core measurements to the atmosphere. We measure air from the SIO pier in La Jolla, CA (which we call La Jolla air) in reference to the working standards while attempting to mimic the ice core analysis to the extent possible. La Jolla air is collected following *Severinghaus et al.* [2003], which broadly follows *Keeling et al.* [1998]. We have modified this method by including an additional pump, which pulls air into a large intake tube, concentrically enclosing a smaller tube that captures the air to be measured. This type of aspirated intake setup was designed to increase airflow into the intake tubes, thereby reducing possible fractionation associated with the initial capture of air [*Blaine*, 2005]. The smaller tube, and the tubing used in this air collection method is ¼" OD Synflex polyethylene-aluminum composite tubing. Connections are made using Ultratorr fittings with Viton O-rings. The air is then pumped at 4 L min^{-1} through two glass water traps at −100°C to remove the water vapor. After it is dried, the air is pumped through ~2 m of tubing to a series of three stainless steel 4-cm^3 volumes, followed by a 2-m tail of tubing to prevent the ambient air from entering the 4-cm^3 volumes. Air is pumped through this setup for 10 min to attain a steady state with respect to possible fractionation. The pump is then stopped abruptly, and after waiting 5 s for airflow to stop, we close the valves on the 4-cm^3 sample volumes.

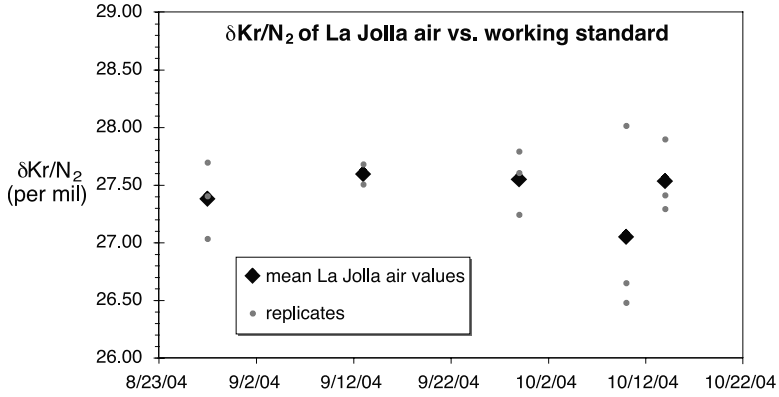

Figure 5. $\delta Kr/N_2$ of La Jolla air (sampled from the SIO pier in La Jolla, CA) measured versus the working standard, over a 2-month period. $\delta Kr/N_2$ is calculated using measured $\delta Kr/Ar$, $\delta^{40}Ar$, and $\delta Ar/N_2$ in La Jolla air. La Jolla air is typically measured in triplicate. The small dots represent the individual replicates, and the bigger diamonds are the mean value for each set of replicates. The standard deviation of the mean values from each set of three replicates is ±0.22‰. The standard deviation of all of the replicates from the entire data set is 0.45‰.

[30] La Jolla air samples are analyzed by the same procedure used for ice analysis, with the exception of air extraction from the ice. Air from the 4-cm^3 sample volume is transferred into a dip tube, which is then run on the Finnigan Delta Plus XP mass spectrometer to measure $\delta^{15}N$, $\delta^{18}O$, $\delta O_2/N_2$, and $\delta Ar/N_2$. After mass spectrometry, air in the sample bellows is refrozen into another dip tube at 4 K. The air in the dip tube is then gettered, enriched with ultrapure N_2, and measured on the Finnigan MAT 252 mass spectrometer to determine the $\delta^{40}Ar$, $\delta Kr/Ar$, and $\delta Xe/Ar$.

[31] La Jolla air is measured regularly throughout a set of ice core measurements, approximately once every two weeks. After they are measured, the La Jolla air values are used to normalize ice core measurements until the next time La Jolla air is measured. The La Jolla air values were relatively constant through the duration of these measurements (Figure 5), with a standard deviation among the $\delta Kr/N_2$ means of 0.22‰ (the standard deviation of the entire data set taken together is 0.44‰). We typically measure La Jolla air in triplicate, using three 4-cm^3 volumes, as described above. We use the mean La Jolla air $\delta Kr/N_2$ value of the three replicates, corrected for pressure imbalance and chemical slope effects, to normalize the $\delta Kr/N_2$ ice core measurements to the atmosphere:

$$\delta Kr/N_2 = \left\{ \left[\left(\delta Kr/N_{2\,\text{measured, corrected}} \right)/10^3 + 1 \right]/ \left[\left(\delta Kr/N_{2\,\text{La Jolla air}} \right)/10^3 + 1 \right] - 1 \right\} \times 10^3‰. \quad (13)$$

This normalization allows us to refer to ice core $\delta Kr/N_2$ in terms of deviation from today's atmosphere.

4. Sources of Fractionation Within the Firn

[32] The top ~50–100 m of an ice sheet is composed of a porous snow layer, called the firn. Air in the firn mixes with the atmosphere mainly through diffusion, and sometimes through convection [*Schwander et al.*, 1993; *Battle et al.*, 1996]. At the bottom of the firn, air is trapped in bubbles, and the firn becomes ice. Processes occurring within the firn can affect the $\delta Kr/N_2$, as well as other gases, and the trapped air reflects these effects.

4.1. Gravitational Fractionation

[33] Gravitational fractionation is one such process that can obscure the accurate representation of the paleoatmosphere. Gravitational settling causes the air in firn and in bubbles that form at the firn/ice transition to preferentially include heavier isotopes. Gravitational fractionation is described by the barometric equation modified for a gas pair [*Craig et al.*, 1988]:

$$R/R_o = e^{gz\Delta m/R^*T}, \quad (14)$$

where R is the isotope or gas ratio measured, R_o is the same ratio in the free atmosphere, g is the local gravitational acceleration, z is the thickness of the firn, Δm is the mass difference between the two isotopes, R^* is the gas constant, and T is the isothermal temperature of the column.

[34] Gravitational fractionation varies in accordance with mass difference, so $\delta^{84}Kr/^{28}N_2$ is 14 times more affected by gravity than $\delta^{40}Ar$ (mass difference of 56 amu compared to a difference of 4 amu) (Figure 6). The measured $\delta^{40}Ar$ value is used to correct $\delta Kr/N_2$ for gravitational fractionation as follows:

$$\delta Kr/N_{2\,\text{gravcorr}} = \delta Kr/N_{2\,\text{measured}} - \delta^{40}Ar \times \Delta m/4. \quad (15)$$

In this case, Δm is the mass difference between ^{84}Kr and $^{28}N_2$, which is 56 amu.

4.2. Gas Loss Fractionation

[35] *Bender et al.* [1995] noted another form of fractionation in ice cores, which they refer to as "configurational" fractionation. After correcting for gravitational fractionation, they found that the elemental ratios O_2/N_2 and Ar/N_2 were significantly lower than atmospheric values. They concluded that gases must have been escaping through small cracks created in the ice cores during drilling and retrieval. Bender et al. found that the mode of gas transport through these cracks could be what they refer to as

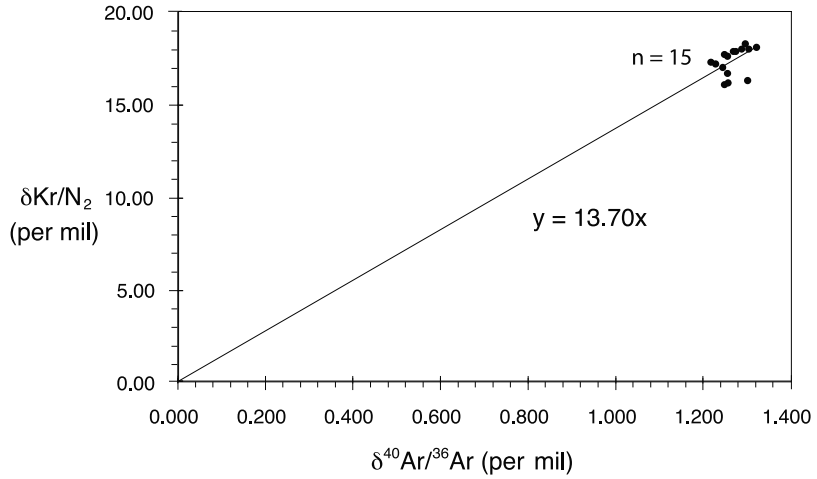

Figure 6. $\delta Kr/N_2$ plotted versus $\delta^{40}Ar/^{36}Ar$ in GISP2 late Holocene ice (140–142 m), n = 15. $\delta Kr/N_2$ is ~14 times $\delta^{40}Ar/^{36}Ar$, as expected because of gravitational fractionation.

configurational fractionation, where molecular diameter controls relative rates of gas loss. According to their analysis, smaller gas molecules were preferentially able to escape through small cracks in the ice.

[36] Further studies have found that gases may also escape from the ice naturally during bubble close-off, causing a similar type of size-dependent fractionation [*Severinghaus and Battle*, 2006; *Bender*, 2002]. Severinghaus and Battle measured Ar/N_2, Ne/N_2, O_2/N_2, Kr/N_2, and Xe/N_2 in firn air from Siple Dome and South Pole, Antarctica. They found enrichments in firn air Ar/N_2, Ne/N_2, O_2/N_2, while the Kr/N_2 and Xe/N_2 data show no enrichment. The O_2/N_2 measured in bubble ice show a complementary depletion, which suggests a process by which smaller molecules preferentially escape from the air bubble as it closes off [*Severinghaus and Battle*, 2006].

[37] This finding may indicate the existence of a threshold molecular size, in which molecules of greater size than the threshold value are not affected by this "close-off" fractionation. The Siple Dome and South Pole firn air data show that the extent of close-off fractionation decreases with increasing molecular diameter, from Ne to O_2 to Ar. Kr and Xe, on the other hand, do not show any enrichment in the firn air. The effective diameter of Kr is 3.64Å, while Ar has a diameter of 3.54Å, suggesting a threshold diameter of ~3.6Å [*Severinghaus and Battle*, 2006].

[38] Kr and N_2 are both larger than this "threshold size," so $\delta Kr/N_2$ measured in air bubbles should not be affected by gas loss fractionation, and hence should represent the abundance of these gases in the paleoatmosphere. However, some ice cores do show variations in Kr/N_2 that correlate with extreme gas loss (deep Byrd core [*Grachev*, 2004]). In this case, $\delta O_2/N_2$ is about −200‰, in contrast to typical values of −5 to −10‰ for well-preserved ice samples [*Bender et al.*, 1995]. Ice having undergone this extreme level of gas loss should not be considered as reliably recording atmospheric Kr/N_2.

5. Results

[39] Ice from the late Holocene part of the GISP2 ice core (gas age ~230 years before present) was analyzed for $\delta Kr/N_2$ as a control test. The mean ocean temperature has not changed substantially between the late Holocene and today, so $\delta Kr/N_2$ measured in air bubbles in ice from the late Holocene should be within error of 0‰ if it is primarily reflecting ocean temperature change. The measured $\delta Kr/N_2$ from this late Holocene ice is +0.07 ± 0.30‰ (n = 16, from 9 depths) for one set of measurements (~146 m), and −0.14 ± 0.93‰ (n = 17, from 6 depths) for another set of measurements (~140.5–142 m) (Figure 3). Here, measurement error is reported as the pooled standard deviation (equation (16)) divided by the square root of the number of replicates. These error calculations are described in detail below. These Holocene $\delta Kr/N_2$ data are all within measurement error of 0‰. The technique thus passes this first-order test.

[40] The $\delta Kr/N_2$ measured in air bubbles from the LGM portion of the GISP2 ice core show a negative shift in their values (Figure 3). The measured $\delta Kr/N_2$ from the LGM is −1.34 ± 0.37‰, which corresponds to a modeled mean ocean temperature change of 2.7 ± 0.6°C between the LGM and today (Figure 1). GISP2 ice core depth for these LGM samples ranged from 1930.00 m to 1932.36 m, which correlates to a ~100 year time span from 20,386 to 20,487 years before 1950 (B.P.) [*Meese et al.*, 1997]. Assuming the gas age–ice age difference is ~860 years [*Severinghaus and Brook*, 1999], the gas ages span the interval 19,500–19,600 years B.P.

[41] We also measured $\delta Xe/N_2$ simultaneously with $\delta Kr/N_2$ in the late Holocene and LGM ice samples. $\delta Xe/N_2$ precision is much poorer than that of $\delta Kr/N_2$. In the late Holocene ice samples (the same as those in which we measured $\delta Kr/N_2$), $\delta Xe/N_2$ values were −0.29 ± 1.71‰ (n = 16, from 9 depths) at ~146 m, and −2.29 ± 3.49‰ (n = 17, from 6 depths) at ~140.5–142 m (Figure 7). $\delta Xe/N_2$ error is calculated in the same way as that of $\delta Kr/N_2$. $\delta Xe/N_2$ measured in ice from the LGM was −6.93 ± 1.83‰, which corresponds to a 4.5 ± 1.0°C temperature change between the LGM and today (Figure 7). We compute this temperature estimate in the same way as for $\delta Kr/N_2$, but using the Xe mole fraction in the atmosphere to estimate $Xe_{present\ atmosphere}$, and Xe solubilities [*Wood and Caputi*, 1966; *Hamme and Severinghaus*, 2007]

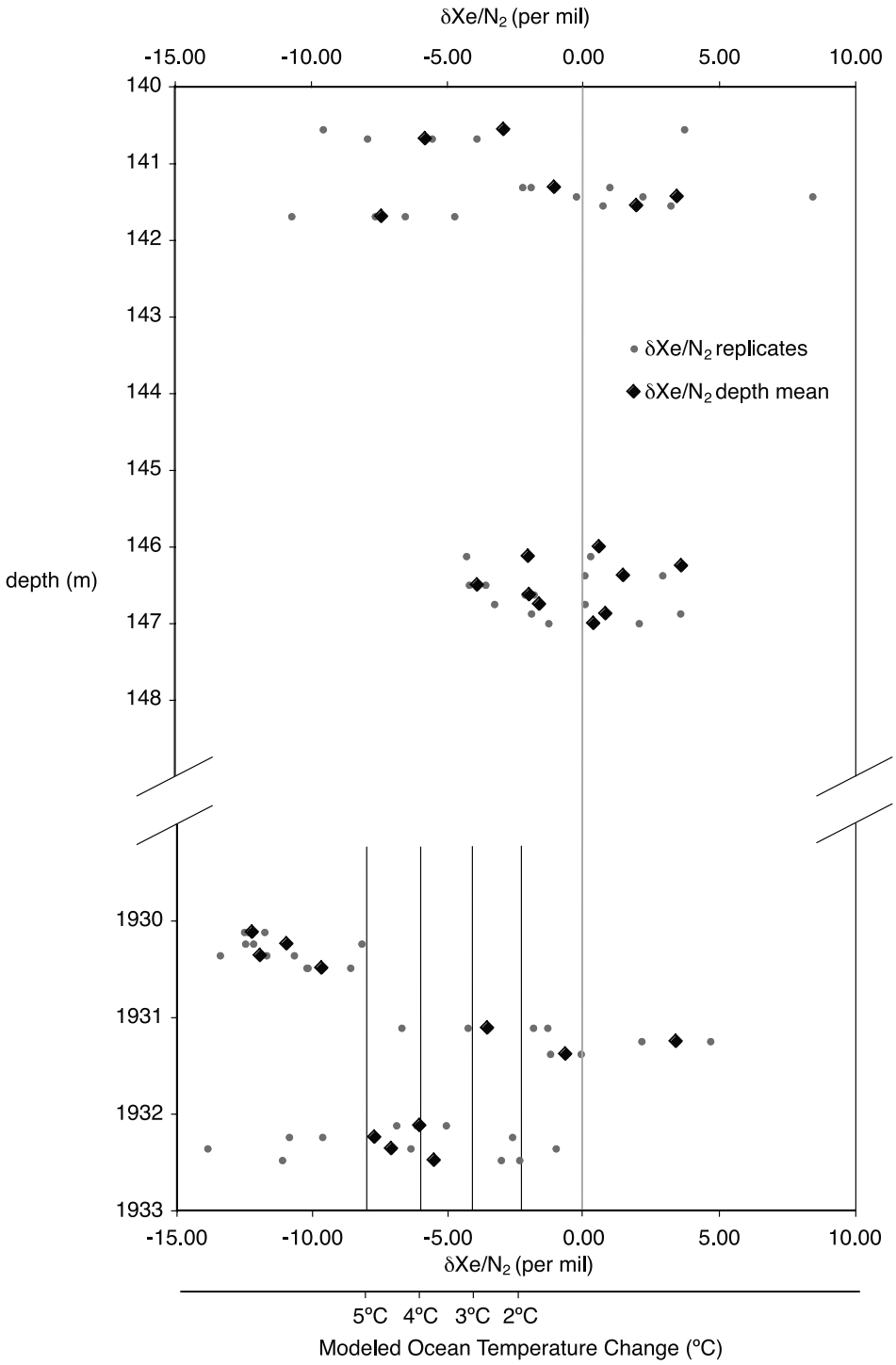

Figure 7. GISP2 ice core depth plotted versus $\delta Xe/N_2$. Vertical axis is not to scale. Long shaded vertical line denotes $\delta Xe/N_2 = 0‰$. Small shaded circles are individual replicates at each depth, and bold solid diamonds are the mean values for each depth. Late Holocene $\delta Xe/N_2$ means are $-0.29 \pm 1.71‰$ (n = 16) at ~146 m, and $-2.29 \pm 3.49‰$ (n = 17) at ~140.5–142 m. Measurement error is reported as the pooled standard deviation (equation (16)) divided by the square root of the number of replicates (three replicates at each depth). The LGM $\delta Xe/N_2$ mean is $-6.93 \pm 1.83‰$ (shown in the bottom portion at 1930–1933 m depths). Short vertical lines are the modeled $\delta Xe/N_2$ resulting from a 2°, 3°, 4°C, and 5°C ΔT mean ocean temperature change.

to estimate $Xe_{present\ ocean}$ and $Xe_{LGM\ ocean}$. The large error in the $\delta Xe/N_2$ Holocene and LGM measurements, as well as the apparent overestimate of temperature change indicated by LGM $\delta Xe/N_2$, are possibly due to analytical problems that are not yet understood. It is also possible that processes such as adsorption/desorption of Xe onto boreal soils could affect the $\delta Xe/N_2$ results. This effect is discussed in the next section. We do not yet understand these $\delta Xe/N_2$ measurements, but with improved precision, they may serve as an additional, independent indicator of ocean temperature change, or they may elucidate other processes affecting the $\delta Kr/N_2$ measurements.

[42] Standard error is calculated using the pooled standard deviation. As defined by *Severinghaus et al.* [2003], pooled standard deviation, s_{pooled}, is the square root of the summed squared deviations of replicates δ_i from their respective means, δ_{jmean}, divided by the degrees of freedom (the number of samples n minus the number of reported means m):

$$s_{pooled} \equiv \left(\frac{\sum_{i,j=1}^{n,m} \left(\delta_i - \overline{\delta_j}\right)^2}{n-m} \right)^{0.5}. \quad (16)$$

Ice samples are measured in duplicate or triplicate, so this calculation is useful because it includes the deviation between replicates from the same depth to compute the overall deviation of the data set. Each depth is typically measured in triplicate, so the standard error is calculated as the pooled standard deviation divided by the square root of the number of replicates (in this case, 3).

[43] As can be seen in Figures 3 and 7, the scatter in the data is large compared to the expected signal. This limits the current utility of the method for paleoclimatic application. However, future improvements in precision are anticipated, and the current work serves as an indication of the method's potential.

6. Discussion

6.1. Processes Affecting $\delta Kr/N_2$ Interpretation

[44] Geothermal heating is one source of heat to the ocean that would not be calculable using atmospheric $\delta Kr/N_2$. $\delta Kr/N_2$ can only record inputs of heat from the surface, whereas geothermal heat enters the ocean at the seafloor. Geothermal heat input (0.05 W/m^2) is generally expected to have a negligible effect on ocean heat content, as its input is much smaller than solar heat flux into the ocean (~200 W/m^2). However, this may not be the case if the ocean were extremely stagnant in the past, allowing heat to build up in the deep ocean [*Adkins et al.*, 2005]. It is believed that the deep ocean was more stagnant in the LGM, as compared to today [*Adkins et al.*, 2002]. If the ocean were stagnant long enough for a substantial amount of geothermal heat to accumulate in the deep ocean, then our $\delta Kr/N_2$ method would overestimate ocean temperature change. Assuming a heat flux of 0.05 W/m^2, we find that the deep ocean would need to be stagnant (or at least to avoid contact with the atmosphere) for 2,500 years for mean ocean temperature to increase by 0.3°C [*Joyce et al.*, 1986]. The temperature change due to geothermal heating in this extreme case is still below the detection limit of the $\delta Kr/N_2$ method presented in this study (0.6°C error). There is no evidence for deep ocean stagnation of such an extent during the LGM, so we conclude that geothermal heating would not bias our LGM ocean temperature estimate significantly.

[45] One last caveat in interpreting atmospheric $\delta Kr/N_2$ as solely reflecting ocean temperature change is the possibility that "sticky" gases like krypton are affected by adsorption/desorption onto boreal soils. This effect would be even more extreme for xenon, which we have measured simultaneously with krypton. Our xenon results have more uncertainty (~2‰), with $\delta Xe/N_2$ shifted to more negative values for both Holocene and LGM measurements (Figure 7). Taking into account this unexplained negative bias, there is still an excess change in $\delta Xe/N_2$ that exceeds the change expected on the basis of the $\delta Kr/N_2$-derived LGM temperature change (Figure 7). It is possible that this difference is caused by net desorption of xenon from cold boreal soils through time from the LGM to the present. Krypton would be less affected than xenon, as xenon is a more adsorptive gas, but it may be affected nonetheless. If this is the case, our temperature change estimate using $\delta Kr/N_2$ may be an upper estimate. We expect to be able to better constrain a possible effect of boreal soils with improved $\delta Xe/N_2$ measurement precision.

6.2. Comparison With Other Deep Ocean Temperature Estimates

[46] The modeled temperature change presented in this paper can be compared with other estimates of deep ocean temperature. *Schrag et al.*'s [1996] pore fluid data from a limited number of sites suggested a deep ocean temperature change of ~4°C, while *Martin et al.* [2002] found a smaller change of ~2.5°C using Mg/Ca of benthic foraminifera. *Waelbroeck et al.* [2002] and *Cutler et al.* [2003] have used a combination of benthic $\delta^{18}O$ ($\delta^{18}O_b$) measurements and coral-based sea level estimates to estimate deep ocean temperatures. In comparing $^{18}O_b$ and coral-derived relative sea level (RSL), *Waelbroeck et al.* [2002] identified two different regression "regimes": one during glaciation, and the other during deglaciation. They used these regressions between RSL and $\delta^{18}O_b$ to estimate deep ocean temperature, assuming a global mean $\Delta\delta^{18}O$ due to ice volume change of 1.1‰. They found that the LGM deep ocean was ~4°C, 3°C, and 2°C colder than today in the North Atlantic, Southern Indian, and Pacific Ocean, respectively, with larger temperature changes possible if $\Delta\delta^{18}O$ due to ice volume is less than 1.1‰. Using a similar method to *Waelbroeck et al.* [2002], *Cutler et al.* [2003] found deep ocean temperature changes of 2°C in the Pacific and 4°C in the Atlantic, using a combination of $\delta^{18}O_b$ and sea level estimates from the Huon Peninsula, Papua New Guinea, and Barbados corals. In comparison to these local estimates of deep ocean temperature change, the mean ocean temperature change of 2.7 ± 0.6°C that we present in this paper appears to be at least a consistent estimate.

[47] This estimate of the mean ocean temperature change between the LGM and today may provide some insight into the change in deep ocean temperature during this time period, which could help constrain previously proposed mechanisms of climate change. *Keeling and Stephens*

[2001] propose a mechanism for Pleistocene climate instability that requires for its operation the cooling of deep ocean waters to virtually the freezing point. The mean ocean temperature change of 2.7 ± 0.6°C that we present here implies that the deep ocean may have been near the freezing point of seawater, but a more precise estimate would place tighter constraints on this hypothesis.

[48] **Acknowledgments.** We thank R. Keeling for suggesting the idea that atmospheric Kr would reflect ocean temperature change, and we thank W. Jenkins, R. Hamme, and K. Kawamura for helpful discussions. R. Beaudette assisted in the laboratory. We thank the staff of the National Ice Core Laboratory for assistance in ice sample handling. This work was supported by NSF grants ATM99-05241 and OPP05-38630.

References

Adkins, J. F., and D. P. Schrag (2001), Pore fluid constraints on deep ocean temperature and salinity during the last glacial maximum, *Geophys. Res. Lett.*, *28*(5), 771–774.

Adkins, J. F., K. McIntyre, and D. P. Schrag (2002), The salinity, temperature, and $\delta^{18}O$ of the glacial deep ocean, *Science*, *298*, 1769–1773.

Adkins, J. F., A. P. Ingersoll, and C. Pasquero (2005), Rapid climate change and conditional instability of the glacial deep ocean from the thermobaric effect and geothermal heating, *Quat. Sci. Rev.*, *24*, 581–594.

Battle, M., et al. (1996), Atmospheric gas concentrations over the past century measured in air from firn at the South Pole, *Nature*, *383*, 231–235.

Bender, M. L. (2002), Orbital tuning chronology for the Vostok climate record supported by trapped gas composition, *Earth Planet. Sci. Lett.*, *204*(1), 275–289.

Bender, M., T. Sowers, and V. Lipenkov (1995), On concentrations of O_2, N_2, and Ar in trapped gases from ice cores, *J. Geophys. Res.*, *100*, 18,651–18,660.

Blaine, T. W. (2005), Continuous measurements of atmospheric argon/nitrogen as a tracer or air-sea heat flux: Models, method, and data, Ph.D. thesis, Univ. of Calif., San Diego, La Jolla.

Craig, H., and R. C. Weins (1996), Gravitational enrichment of $^{84}Kr/^{36}Ar$ ratios in polar ice caps: a measure of firn thickness and accumulation temperature, *Science*, *271*, 1708–1711.

Craig, H., Y. Horibe, and T. Sowers (1988), Gravitational separation of gases and isotopes in polar ice caps, *Science*, *242*, 1675–1678.

Crowley, T. J., and G. R. North (1991), *Paleoclimatology*, Oxford Univ. Press, New York.

Cutler, K. B., R. L. Edwards, F. W. Taylor, H. Cheng, J. Adkins, C. D. Gallup, P. M. Cutler, G. S. Burr, and A. L. Bloom (2003), Rapid sea-level fall and deep-ocean temperature change since the last interglacial period, *Earth Planet. Sci. Lett.*, *206*, 253–271.

Egbert, G. D., R. D. Ray, and B. G. Bills (2004), Numerical modeling of global semidiurnal tide in the present day and in the last glacial maximum, *J. Geophys. Res.*, *109*, C03003, doi:10.1029/2003JC001973.

Fairbanks, R. G. (1989), A 17,000-year glacio-eustatic sea level record; influence of glacial melting rates on the Younger Dryas event and deep-ocean circulation, *Nature*, *342*, 637–642.

Grachev, A. M. (2004), Laboratory-determined air thermal diffusion constants applied to reconstructing the magnitudes of past abrupt temperature changes from gas isotope observations in polar ice cores, Ph.D. thesis, Univ. of Calif., San Diego, La Jolla.

Hamme, R. C., and S. R. Emerson (2002), Mechanisms controlling the global oceanic distribution of inert gases argon, nitrogen, and neon, *Geophys. Res. Lett.*, *29*(23), 2120, doi:10.1029/2002GL015273.

Hamme, R. C., and J. P. Severinghaus (2007), Trace gas disequilibria during deep-water formation, *Deep Sea Res., Part I*, *54*, 939–950.

Joyce, T. M., B. A. Warren, and L. D. Talley (1986), The geothermal heating of the abyssal subarctic Pacific Ocean, *Deep Sea Res., Part A*, *33*(8), 1003–1015.

Keeling, R. F., and B. B. Stephens (2001), Antarctic sea ice and the control of Pleistocene climate instability, *Paleoceanography*, *16*, 112–131.

Keeling, R. F., A. C. Manning, E. M. McEvoy, and S. R. Shertz (1998), Methods for measuring changes in atmospheric O_2 concentration and their application in southern hemisphere air, *J. Geophys. Res.*, *103*(D3), 3381–3397.

Levitus, S. (1994), *World Ocean Atlas*, NOAA, Washington D. C.

Martin, P. M., D. W. Lea, Y. Rosenthal, N. J. Shackleton, M. Sarnthein, and T. Papenfuss (2002), Quaternary deep sea temperature histories derived from benthic foraminiferal Mg/Ca, *Earth Planet. Sci. Lett.*, *198*, 193–209.

Meese, D. A., A. J. Gow, R. B. Alley, G. A. Zielinski, P. M. Grootes, M. Ram, K. C. Taylor, P. A. Mayewski, and J. F. Bolzan (1997), The Greenland Ice Sheet Project 2 depth-age scale: Methods and results, *J. Geophys. Res.*, *102*, 26,411–26,423.

Schlesinger, W. H. (1997), *Biogeochemistry, An Analysis of Global Change*, 2nd ed., Academic, San Diego, Calif.

Schrag, D. P., G. Hampt, and D. W. Murray (1996), Pore fluid constraints on the temperature and oxygen isotopic composition of the glacial ocean, *Science*, *272*, 1930–1932.

Schwander, J., J.-M. Barnola, C. Andrie, M. Leuenberger, A. Ludin, D. Raynaud, and B. Stauffer (1993), The age of the air in the firn and the ice at Summit, Greenland, *J. Geophys. Res.*, *98*, 2831–2838.

Severinghaus, J. P., and M. O. Battle (2006), Fractionation of gases in polar ice during bubble close-off: New constraints from firn air Ne, Kr, and Xe observations, *Earth Planet. Sci. Lett.*, *244*, 474–500.

Severinghaus, J. P., and E. J. Brook (1999), Abrupt climate change at the end of the last glacial period inferred from trapped air in polar ice, *Science*, *286*, 930–934.

Severinghaus, J. P., B. Luz, and N. Caillon (2003), A method for precise measurement of argon 40/36 and krypton/argon ratios in trapped air in polar ice with applications to past firn thickness and abrupt climate change in Greenland and at Siple Dome, Antarctica, *Geochim. Cosmochim. Acta*, *67*(3), 325–343.

Shackleton, N. J. (2000), The 100,000 year ice-age cycle identified and found to lag temperature, carbon dioxide, and orbital eccentricity, *Science*, *289*, 1897–1902.

Sowers, T., and M. L. Bender (1995), Climate records covering the last deglaciation, *Science*, *269*, 210–214.

Sowers, T., M. L. Bender, and D. Raynaud (1989), Elemental and isotopic composition of occluded O_2 and N_2 in polar ice, *J. Geophys. Res.*, *94*, 5137–5150.

Waelbroeck, C., L. Labeyrie, E. Michel, J. C. Duplessy, J. F. McManus, K. Lambeck, E. Balbon, and M. Labracherie (2002), Sea-level and deep water temperature changes derived from benthic foraminifera isotopic records, *Quat. Sci. Rev.*, *21*, 295–305.

Watson, A. J., and A. C. N. Garbato (2006), The role of Southern Ocean mixing and upwelling in glacial-interglacial atmospheric CO_2 change, *Tellus, Ser. B*, *58*, 73–87.

Weiss, R. F. (1970), The solubility of nitrogen, oxygen and argon in water and sea water, *Deep Sea Res.*, *17*, 721–735.

Weiss, R. F., and T. K. Kyser (1978), Solubility of krypton in water and seawater, *J. Chem. Eng. Data*, *23*(1), 69–72.

Wood, D., and R. Caputi (1966), Solubilities of Kr and Xe in fresh and seawater, *Tech. Rep. USNRDL-TR-988*, U.S. Nav. Radiol. Def. Lab., San Francisco, Calif.

M. A. Headly and J. P. Severinghaus, Scripps Institution of Oceanography, University of California, San Diego, 9500 Gilman Drive, La Jolla, CA 92093, USA. (mheadly@ucsd.edu)